ANALYTICAL STUDY OF DELAMINATION IN MULTILAYERED TWO-DIMENSIONAL FUNCTIONALLY GRADED NON-LINEAR ELASTIC BEAMS

V. I. Rizov*

Department of Technical Mechanics
University of Architecture, Civil Engineering and Geodesy
Sofia, Bulgaria

ABSTRACT

The present paper is focused on the delamination fracture in a multilayered two-dimensional functionally graded beam configuration which exhibits non-linear behavior of the material. The beam is loaded by two longitudinal forces applied at the beam free ends. The beam contains a delamination crack which is located symmetrically with respect to the beam mid-span. The delamination is studied analytically in terms of the strain energy release rate. The *J*-integral approach is applied for verification of the analysis of the strain energy release rate. The solution derived is valid for a beam made of an arbitrary number of layers. It is assumed that each layer has individual thickness and material properties. Also, the material is two-dimensional functionally graded in the cross-section of each layer. The solution obtained can be applied for a delamination crack located arbitrary along the height of the beam cross-section. It is shown that the solution is very convenient for investigating the influences of material gradients and crack location on the delamination fracture behavior. The results obtained can be used for optimization of multilayered two-dimensional functionally graded structural members and components with respect to their delamination fracture performance.

Keywords: Functionally graded beam, Multilayered structure, Delamination, Material non-linearity.

1. INTRODUCTION

The functionally graded materials have found various applications in many engineering areas (aeronautics, electronics, optics, defense industries, car manufacture and biomedical sectors) in recent years [1-11]. This is own mainly to their superior mechanical and thermal properties in comparison with the traditional structural materials. The functionally graded materials are new inhomogeneous materials made by mixing of two material constituents. One of the characteristic properties of the functionally graded materials is the fact that the volume fractions of material constituents vary continuously in one or more spatial coordinates. In this way, one can modify the composition of the functionally graded material during manufacturing, so as to satisfy requirements for different material properties in different parts of a member.

The evaluation of the reliability and integrity of functionally graded structural members requires profound knowledge of their fracture behavior since cracks reduce considerably the strength and stiffness and can lead to failure of the whole structure. Therefore, great efforts have been devoted to study the fracture in functionally graded materials [12-20].

Studies of fracture behavior of functionally graded materials subjected to static or fatigue crack loading conditions have been reviewed in [13]. The effects of mechanical properties on the fracture have been discussed. Publications dealing with cracks parallel and perpendicular to the material gradient direction have been presented. Various analyses of fracture by applying methods of linear-elastic fracture mechanics have been considered. Investigations of circular arc cracks and slightly curved cracks have also been reviewed. Studies of the fatigue fracture behavior under cyclic loading have been summarized. The influence of thermal loading on the fracture in functionally graded materials has been discussed.

Theoretical fracture analyses of functionally graded materials have been carried-out in [14]. Linear-elastic behavior of the material has been assumed. An engineering method for predicting the strength of structural members composed by functionally graded materials incorporating re-entrant corners has been developed. It has been assumed that the strength corresponds to the

* Corresponding author (V_RIZOV_FHE@UACG.BG)

DOI : 10.1017/jmech.2017.104
Copyright © 2017 The Society of Theoretical and Applied Mechanics
https://doi.org/10.1017/jmech.2017.104 Published online by Cambridge University Press

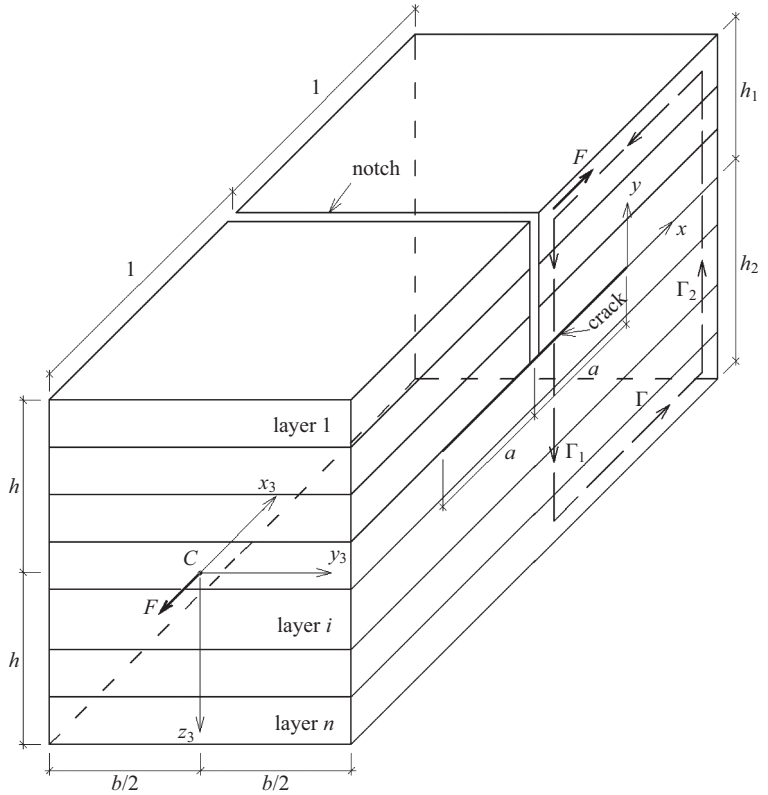


Fig. 1 Geometry and loading of a multilayered two-dimensional functionally graded beam.

unstable brittle crack propagation. The validity of the method has been proved by analyzing functionally graded members (plates loaded in tension and beams under three-point bending) containing re-entrant corners. The effects of corner-angle and depth have been discussed.

Cracked functionally graded beams under three-point bending have been analyzed by applying the compliance approach [15]. Equivalent homogeneous beams of variable height for the cracked functionally graded beams have been suggested. Beams containing cracks of different lengths have been investigated assuming linear-elastic behaviour of the material. The compliance characteristics have been obtained by applying different laws for height variation of the equivalent beams. It has been found that besides for three-point bending beams, the equivalent compliance concept is suitable also for analyzing fracture behaviour of functionally graded structural members and components loaded by concentrated loads.

Dynamic analyses of cracked functionally graded beams have been performed in [16]. Clamped-clamped and clamped-free beam configurations have been considered. Vibration behaviour has been investigated for different crack locations and crack depths. Cracked beams have been modelled as two sub-beams connected by a mass-less rotational spring. Continuity of the longitudinal and transverse displacements in the cracked section is assumed. However, discontinuity in the rotational displacement has been taken into account in the modelling. It has been assumed that the material is functionally graded in the thickness direction. Frequencies and mode shapes which correspond to the first three modes of free vibration of the cracked beams have been determined.

Multilayered materials represent an important class of inhomogeneous materials [21-26]. Due to their high strength-to-weight and stiffness-to-weight ratios, multilayered materials have been widely used in various structural components. Delamination cracking, i.e. separation of layers, is one of the most dangerous failure modes in multilayered structural members [27-31].

The main purpose of the present paper is to analyze the delamination fracture in multilayered two-dimensional functionally graded beams which exhibit non-linear mechanical behavior of the material. The fracture is studied analytically in terms of the strain energy release rate. The *J*-integral approach is applied in order to verify the solution for the strain energy release rate derived in the present paper. The influence of crack location along the height of the beam cross-section and material gradients on the delamination fracture behavior is investigated. The results obtained can be applied to optimize the multilayered two-dimensional functionally graded beam structures with respect to delamination fracture performance in their design stage.

2. FRACTURE ANALYSIS

The present paper deals with delamination fracture analyses of the multilayered two-dimensional functionally graded beam configuration shown schematically in Fig. 1. The beam is made of an arbitrary number of layers. Each layer has individual thickness and material

https://doi.org/10.1017/jmech.2017.104 Published online by Cambridge University Press

properties. Perfect adhesion is assumed between layers. The beam has a rectangular cross-section of width, b, and height, $2h$. The external loading consists of two longitudinal forces, F, applied at the free ends of the beam as shown in Fig. 1. A vertical notch of depth, h_2, is introduced in the beam mid-span in order to generate conditions for delamination fracture. A delamination crack of length, $2a$, is located symmetrically with respect to the beam mid-span. The thicknesses of the lower and upper crack arms are marked by h_1 and h_2, respectively. It is obvious that the upper crack arm is free of stresses (Fig. 1). The material is two-dimensional functionally graded in the cross-section of each layer. Besides, the material exhibits non-linear mechanical behavior.

Due to the symmetry, only half of the beam, $l \le x_3 \le 2l$, is considered in the analysis (Fig. 1).

The delamination fracture is studied in terms of the strain energy release rate, G, which is defined as

$$G = \frac{dW_{ext} - dU}{dA}, \tag{1}$$

where the increase of the crack area, dA, is written as

$$dA = bda. \tag{2}$$

In formula (1), dW_{ext} and dU are the changes of the external work and the strain energy, respectively. In (2), da is an elementary increase of the crack length.

Since the change of the external work can be expressed as

$$dW_{ext} = dU + dU^*, \tag{3}$$

formula (1) takes the form

$$G = \frac{dU^*}{bda}, \tag{4}$$

where dU^* is the change of the complementary strain energy of the beam.

It should be noted that the present analysis holds for non-linear elastic behavior of the material. The analysis is applicable also for elastic-plastic behavior of the material if the beam undergoes active deformation, i.e. if the external loading increases only [32, 33]. Besides, the present analysis is based on the small strains assumption.

The complementary strain energy cumulated in half of the beam is obtained as

$$U^* = U_L^* + U_U^*, \tag{5}$$

where U_L^* and U_U^* are, respectively, the complementary strain energies in the lower crack arm, $l \le x_3 \le l + a$, and the un-cracked beam portion, $l + a \le x_3 \le 2l$.

The complementary strain energy in the lower crack arm is written as

$$U_L^* = a \sum_{i=1}^{i=n_L} \iint_{A_i} u_{0L_i}^* dA_i, \tag{6}$$

where n_L is the number of layers in the lower crack arm (Fig. 2), $u_{0L_i}^*$ is the complementary strain energy density distribution in the cross-section of the i-th layer, A_i is the area of cross-section of this layer.

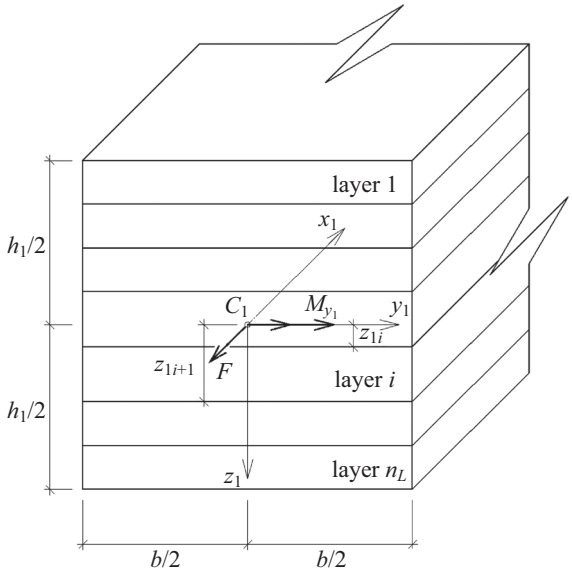


Fig. 2 Schematic representation of the cross-section of the lower crack arm.

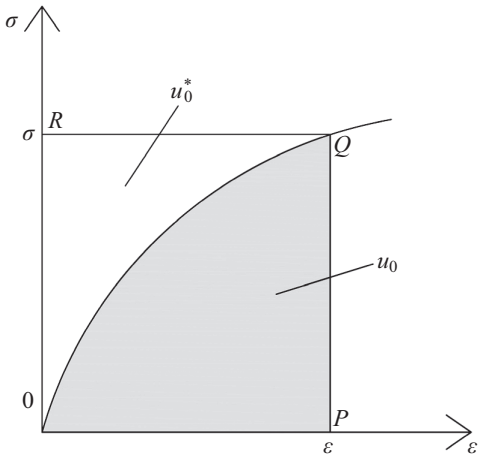


Fig. 3 Non-linear stress-strain curve (the strain energy and the complementary strain energy densities are marked by u_0 and u_0^*, respectively).

In principle, the complementary strain energy density is equal to the area OQR that supplements the area OPQ, enclosed by the stress-strain curve, to a rectangle (Fig. 3). Thus, the complementary strain energy density in the i-th layer of the lower crack is written as

$$u_{0L_i}^* = \sigma_i \varepsilon - u_{0L_i}. \tag{7}$$

In (7), σ_i is the distribution of the longitudinal normal stresses in the cross-section of the i-th layer, ε is the distribution of longitudinal strains, u_{0Li} is the distribution of strain energy density in the cross-section of this layer.

The strain energy density is equal to the area OPQ,

https://doi.org/10.1017/jmech.2017.104 Published online by Cambridge University Press

enclosed by the stress-strain curve (Fig. 3). Hence, u_{0Li} is obtained as

$$u_{0L_i} = \int_0^{\varepsilon} \sigma_i(\varepsilon) d\varepsilon \tag{8}$$

The mechanical behavior of the material in the i-th layer is described by the following non-linear stress-strain relation [34]:

$$\sigma_i = \frac{E_i \varepsilon}{\sqrt{1+\left(\frac{\varepsilon}{t}\right)^2}} \tag{9}$$

where E_i and t are material properties (usually, t is equal to unit [34]).

By combining of (8) and (9), one arrives at

$$u_{0L_i} = E_i t^2 \left[\sqrt{1+\left(\frac{\varepsilon}{t}\right)^2} - 1 \right]. \tag{10}$$

By substituting of (9) and (10) in (7), one derives

$$u^*_{0L_i} = E_i t^2 \left[1 - \frac{1}{\sqrt{1+\left(\frac{\varepsilon}{t}\right)^2}} \right]. \tag{11}$$

The material property, E_i, varies continuously in the cross-section the i-th layer according to the following cubic law:

$$E_i = E_{B_i} + \frac{E_{D_i} - E_{B_i}}{b^3}\left(\frac{b}{2} + y_1\right)^3 + \frac{E_{H_i} - E_{B_i}}{\left(z_{1i+1} - z_{1i}\right)^3}\left(z_1 - z_{1i}\right)^3, \tag{12}$$

where

$$-\frac{b}{2} \le y_1 \le \frac{b}{2}, \quad z_{1i} \le z_1 \le z_{1i+1}, \quad i = 1, 2, ..., n_L. \tag{13}$$

In (12), E_{B_i}, E_{D_i} and E_{H_i} are material properties of the two-dimensional functionally graded material (E_{D_i} and E_{H_i} govern material gradients along the width and thickness of the i-th layer, respectively), z_{1i} and z_{1i+1} are, respectively, the coordinates of the upper and lower surfaces of the i-th layer (Fig. 2), y_1 and z_1 are the centroidal axes of the cross-section of the lower crack arm (Fig. 2).

The distribution of the longitudinal strains is analyzed by applying the Bernoulli's hypothesis for plane sections since the span to height ratio of the beam under consideration is large. Concerning the distribution of the longitudinal strains, it should also be mentioned that since the lower crack arm is loaded in eccentric tension, the only non-zero strain is ε. Therefore, according to the small strains compatibility equations, ε is distributed linearly in the cross-section of the lower crack arm. Thus, ε in the lower crack arm is written as

$$\varepsilon = \varepsilon_{C_1} + \kappa_{y_1} y_1 + \kappa_{z_1} z_1, \tag{14}$$

where ε_{C_1} is the strain in the centre of the lower crack arm cross-section, κ_{y_1} and κ_{z_1} are the curvatures of lower crack arm in the x_1y_1 and x_1z_1 planes, respectively.

The following equations for equilibrium of the lower crack arm cross-section are applied in order to determine ε_{C_1}, κ_{y_1} and κ_{z_1}:

$$N_1 = \sum_{i=1}^{i=n_L} \iint_{A_i} \sigma_i dA_i, \tag{15}$$

$$M_{y_1} = \sum_{i=1}^{i=n_L} \iint_{A_i} \sigma_i z_1 dA_i, \tag{16}$$

$$M_{z_1} = \sum_{i=1}^{i=n_L} \iint_{A_i} \sigma_i y_1 dA_i, \tag{17}$$

where N_1, M_{y_1} and M_{z_1} are the axial force and bending moments about y_1 and z_1 axes, respectively. It can be observed in Fig. 1 and Fig. 2 that

$$N_1 = F, \quad M_{y_1} = F\left(h - \frac{h_1}{2}\right), \quad M_{z_1} = 0. \tag{18}$$

By substituting of (9), (12) and (14) in (15), (16) and (17), one obtains

$$\begin{aligned} N_1 = {} & \lambda_i b\left(\varepsilon_{C_1}\varphi_i + \frac{1}{12}\kappa_{y_1}\eta_i b^2 + \varepsilon_{C_1}\omega_i\frac{b^2}{12}\right) \\ & + \mu_i\frac{b}{2}\left(\kappa_{z_1}\varphi_i + \varepsilon_{C_1}\rho_1 + \frac{b^2}{12}\kappa_{z_1}\omega_i + \frac{b^2}{12}\kappa_{y_1}\gamma_i\right) \\ & + \phi_i\frac{b}{3}\left(\kappa_{z_1}\rho_i + \varepsilon_{C_1}\zeta_i\right) + \kappa_{z_1}\zeta_i\frac{b}{4}\upsilon_i, \end{aligned} \tag{19}$$

$$\begin{aligned} M_{y_1} = {} & \mu_i\frac{b}{2}\left(\varepsilon_{C_1}\varphi_i + \frac{b^2}{12}\kappa_{y_1}\eta_i + \frac{b^2}{12}\varepsilon_{C_1}\omega_i\right) \\ & + \phi_i\frac{b}{3}\left(\kappa_{z_1}\varphi_i + \varepsilon_{C_1}\rho_i + \frac{b^2}{12}\kappa_{z_1}\omega_i + \frac{b^2}{12}\kappa_{y_1}\gamma_i\right) \\ & + \frac{b}{4}\upsilon_i\left(\kappa_{z_1}\rho_i + \varepsilon_{C_1}\zeta_i\right) + \frac{b}{5}\kappa_{z_1}\zeta_i\vartheta_i, \end{aligned} \tag{20}$$

$$\begin{aligned} M_{z_1} = {} & \lambda_i\frac{b^3}{4}\left(\frac{1}{3}\kappa_{y_1}\varphi_i + \frac{1}{3}\varepsilon_{C_1}\eta_i + \frac{b^2}{20}\kappa_{y_1}\omega_i\right) \\ & + \frac{b^3}{24}\mu_i\left(\kappa_{z_1}\eta_i + \kappa_{y_1}\rho_i + \varepsilon_{C_1}\gamma_i\right) \\ & + \frac{b^3}{36}\phi_i\left(\kappa_{z_1}\gamma_i + \kappa_{y_1}\zeta_i\right), \end{aligned} \tag{21}$$

where

$$\psi = \sqrt{1+\frac{\varepsilon_{C_1}^2}{t^2}}, \tag{22}$$

https://doi.org/10.1017/jmech.2017.104 Published online by Cambridge University Press

$$\beta_i = \frac{E_{D_i} - E_{B_i}}{b^3}, \tag{23}$$

$$\delta_i = \frac{E_{H_i} - E_{B_i}}{\left(z_{1i+1} - z_{1i}\right)^3}, \tag{24}$$

$$\theta_i = E_{B_i} + \frac{b^3}{8}\beta_i - \delta_i z_{1i}^3, \tag{25}$$

$$\eta_i = \frac{3\beta_i b}{4\psi} - \frac{\theta_i \varepsilon_{C_1} \kappa_{y_1}}{t^2 \psi^3}, \tag{26}$$

$$\rho_i = \frac{3\delta_i z_{1i}^2}{\psi} - \frac{\theta_i \varepsilon_{C_1} \kappa_{z_1}}{t^2 \psi^3}, \tag{27}$$

$$\begin{aligned}\omega_i =& \frac{3\beta_i b}{2\psi} - \frac{3\beta_i b^2 \varepsilon_{C_1} \kappa_{y_1}}{8t^2\psi^3} \\ & - \frac{\kappa_{y_1}}{2t^2}\left[\left(\frac{3}{4}\beta_i b^2 \varepsilon_{C_1} + E_{B_i}\kappa_{y_1} + \frac{1}{8}\beta_i b^3 \kappa_{y_1} - \delta_i z_{1i}^3 \kappa_{y_1}\right)\frac{1}{\psi^3}\right. \\ & \left. -3\left(E_{B_i}\varepsilon_{C_1} + \frac{1}{8}\beta_i b^3 \varepsilon_{C_1} - \delta_i z_{1i}^3 \varepsilon_{C_1}\right)\frac{\varepsilon_{C_1}\kappa_{y_1}}{t^2\psi^5}\right],\end{aligned} \tag{28}$$

$$\begin{aligned}\gamma_i =& -\frac{3\beta_i b^2 \varepsilon_{C_1} \kappa_{z_1}}{4t^2\psi^3} \\ & - \frac{\kappa_{y_1}}{t^2}\left[\left(3\delta_i z_{1i}^2 \varepsilon_{C_1} + E_{B_i}\kappa_{Z_1} + \frac{1}{8}\beta_i b^3 \kappa_{z_1} - \delta_i z_{1i}^3 \kappa_{z_1}\right)\frac{1}{\psi^3}\right. \\ & \left. -3\left(E_{B_i}\varepsilon_{C_1} + \frac{1}{8}\beta_i b^3 \varepsilon_{C_1} - \delta_i z_{1i}^3 \varepsilon_{C_1}\right)\frac{\varepsilon_{C_1}\kappa_{z_1}}{t^2\psi^5}\right],\end{aligned} \tag{29}$$

$$\begin{aligned}\zeta_i =& -\frac{3\delta_i z_{1i}}{\psi} - \frac{3\delta_i z_{1i}^2 \varepsilon_{C_1} \kappa_{z_1}}{2t^2\psi^3} - \\ & \frac{\kappa_{z_1}}{2t^2}\left[\left(3\delta_i z_{1i}^2 \varepsilon_{C_1} + E_{B_i}\kappa_{z_1} + \frac{1}{8}\beta_i b^3 \kappa_{z_1} - \delta_i z_{1i}^3 \kappa_{z_1}\right)\frac{1}{\psi^3}\right. \\ & \left. -3\left(E_{B_i}\varepsilon_{C_1} + \frac{1}{8}\beta_i b^3 \varepsilon_{C_1} - \delta_i z_{1i}^3 \varepsilon_{C_1}\right)\frac{\varepsilon_{C_1}\kappa_{z_1}}{t^2\psi^5}\right],\end{aligned} \tag{30}$$

$$\varphi_i = \frac{\theta_i}{\psi}, \tag{31}$$

$$\lambda_i = z_{1i+1} - z_{1i}, \tag{32}$$

$$\mu_i = z_{1i+1}^2 - z_{1i}^2, \tag{33}$$

$$\phi_i = z_{1i+1}^3 - z_{1i}^3, \tag{34}$$

$$\upsilon_i = z_{1i+1}^4 - z_{1i}^4, \tag{35}$$

$$\vartheta_i = z_{1i+1}^5 - z_{1i}^5. \tag{36}$$

Equations (19), (20) and (21) should be solved with respect to ε_{C_1}, κ_{y_1} and κ_{z_1} by using the MatLab computer program.

By substituting of (11), (12) and (14) in (6), one derives

$$\begin{aligned}U_L^* =& \sum_{i=1}^{i=n_L} a\left[t^2 b\lambda_i\left(E_{B_i} + \beta_i\frac{b^3}{4} - \varphi_i - \omega_i\frac{b^2}{12}\right)\right. \\ & \left. + t^2 b\frac{\delta_i}{4}\lambda_i^4 - t^2 b\frac{\rho_i}{2}\mu_i - t^2 b\frac{\zeta_i}{3}\phi_i\right].\end{aligned} \tag{37}$$

Formula (37) can be applied also to determine the complementary strain energy, U_U^*, in the un-cracked beam portion. For this purpose, n_L, a, λ_i, φ_i, δ_i, ρ_i, ω_i, μ_i, ϕ_i and ζ_i have to be replaced, respectively, with n, $l–a$, λ_{Ui}, φ_{Ui}, δ_{Ui}, ρ_{Ui}, ω_{Ui}, μ_{Ui}, ϕ_{Ui} and ζ_{Ui}, where n is the number of layers in the un-cracked beam portion. Besides, instead by a, the term in square brackets in (37) has to be multiplied by $l–a$. The quantities, λ_{Ui}, φ_{Ui}, δ_{Ui}, ρ_{Ui}, ω_{Ui}, μ_{Ui}, ϕ_{Ui} and ζ_{Ui} can be determined by formulae (32), (31), (24), (27), (28), (33), (34) and (30), respectively. For this purpose, z_{1i}, z_{1i+1}, ε_{C_1}, κ_{y_1} and κ_{z_1} have to be replaced, respectively, with z_{2i}, z_{2i+1}, ε_{C_2}, κ_{y_2} and κ_{z_2}, where z_{2i} and z_{2i+1} are the coordinates of the upper and lower surfaces of the i-th layer in the un-cracked beam portion, ε_{C_2} is the strain in the centre of the beam cross-section, κ_{y_2} and κ_{z_2} are the beam curvatures in the x_2y_2 and x_2z_2 planes. Analogous replacements have to be done in the equilibrium equations (19), (20) and (21) in order to use these equations to determine ε_{C_2}, κ_{y_2} and κ_{z_2}. Besides, $M_{y_1} = 0$ has to be substituted in equation (20).

Finally, by substituting of U_L^*, U_U^* and (5) in (4) and doubling the expression obtained because of the symmetry (Fig. 1), one derives

$$\begin{aligned}G =& 2t^2\sum_{i=1}^{i=n_L}\left[\lambda_i\left(E_{B_i} + \beta_i\frac{b^3}{4} - \varphi_i - \omega_i\frac{b^2}{12}\right)\right. \\ & \left. + \frac{\delta_i}{4}\lambda_i^4 - \frac{\rho_i}{2}\mu_i - \frac{\zeta_i}{3}\phi_i\right] \\ & - 2t^2\sum_{i=1}^{i=n}\left[\lambda_{U_i}\left(E_{B_i} + \beta_i\frac{b^3}{4} - \varphi_{U_i} - \omega_{U_i}\frac{b^2}{12}\right)\right. \\ & \left. + \frac{\delta_{U_i}}{4}\lambda_{U_i}^4 - \frac{\rho_{U_i}}{2}\mu_{U_i} - \frac{\zeta_{U_i}}{3}\phi_{U_i}\right].\end{aligned} \tag{38}$$

Formula (38) expresses the strain energy released rate in the multilayered two-dimensional functionally graded beam configuration shown in Fig. 1 when the mechanical behavior and the distribution of material property are described by formulae (9) and (12), respectively.

The strain energy release rate (38) is compared with the J-integral [35] for verification. The J-integral is solved by using integration contour, Γ, which coincides with the contour of the right-hand half of the beam in view of the symmetry (Fig. 1). Apparently, the J-integral has non-zero values in only in segments, Γ_1 and Γ_2, of the integration contour (Γ_1 and Γ_2 coincide with the cross-section of the lower crack arm in the beam mid-span and the right-hand free end of the beam, respectively). Hence, the J-integral solution is found by summation of J_{Γ_1} and J_{Γ_2}

https://doi.org/10.1017/jmech.2017.104 Published online by Cambridge University Press

$$J = 2(J_{\Gamma_1} + J_{\Gamma_2}), \tag{39}$$

where J_{Γ_1} and J_{Γ_2} are the J-integral values in segments Γ_1 and Γ_2, respectively. The term in brackets in (39) is doubled because of the symmetry (Fig. 1).

First, the integration is performed in segment, Γ_1, of the integration contour. The J-integral in segment, Γ_1, is written as

$$J_{\Gamma_1} = \sum_{i=1}^{n_L} \int_{z_{1i}}^{z_{1i+1}} \left[u_{0L_i} \cos\alpha - \left(p_{xi} \frac{\partial u}{\partial x} + p_{yi} \frac{\partial v}{\partial x} \right) \right] ds, \tag{40}$$

where α is the angle between the outwards normal vector to the contour of integration and the crack direction, p_{xi} and p_{yi} are the components of stress vector in the i-th layer of the lower crack arm, u and v are the components of displacement vector with respect to the crack tip coordinate system xy (x is directed along the crack), ds is a differential element along the contour.

The components of the J-integral in segment, Γ_1, are written as

$$p_{xi} = -\sigma_i, \tag{41}$$

$$p_{yi} = 0, \tag{42}$$

$$ds = dz_1, \tag{43}$$

$$\cos\alpha = -1, \tag{44}$$

where coordinate, z_1, varies in the interval $[-h_1/2, h_1/2]$. The partial derivative, $\partial u/\partial x$, in (40) is obtained as

$$\frac{\partial u}{\partial x} = \varepsilon = \varepsilon_{C_1} + \kappa_{y_1} y_1 + \kappa_{z_1} z_1, \tag{45}$$

where ε_{C_1}, κ_{y_1} and κ_{z_1} are determined from the equilibrium equations (19), (20) and (21).

By substituting of (9), (10), (41)-(44) and (45) in (40), one derives

$$J_{\Gamma_1} = t^2 \sum_{i=1}^{i=n_L} \left\{ \lambda_i \left[E_{B_i} + \beta_i \left(\frac{b}{2} + y_1 \right)^3 - \varphi_i - \eta_i y_1 - \omega_i y_1^2 \right] + \frac{\delta_i}{4} \lambda_i^4 - \frac{\mu_i}{2} (\rho_i + \gamma_i y_1) - \frac{\zeta_i}{3} \phi_i \right\}, \tag{46}$$

where the coordinate, y_1, varies in the interval $[-b/2, b/2]$.

Formula (46) can also be used to obtain the J-integral solution in segment, Γ_2, of the integration contour (Fig. 1). For this purpose, n_L, λ_i, φ_i, η_i, ω_i, δ_i, μ_i, ρ_i, γ_i, ζ_i and ϕ_i have to be replaced with n, λ_{U_i}, φ_{U_i}, η_{U_i}, ω_{U_i}, δ_{U_i}, μ_{U_i}, ρ_{U_i}, γ_i, ζ_{U_i} and ϕ_{U_i}, respectively. Besides, the sign of (46) must be set to "minus" because the integration contour is directed upwards in segment, Γ_2.

By substituting of J_{Γ_1} and J_{Γ_2} in (39), one arrives at

$$J_{\Gamma_1} = 2t^2 \sum_{i=1}^{i=n_L} \left\{ \lambda_i \left[E_{B_i} + \beta_i \left(\frac{b}{2} + y_1 \right)^3 - \varphi_i - \eta_i y_1 - \omega_i y_1^2 \right] + \frac{\delta_i}{4} \lambda_i^4 - \frac{\mu_i}{2} (\rho_i + \gamma_i y_1) - \frac{\zeta_i}{3} \phi_i \right\} - 2t^2 \sum_{i=1}^{i=n} \left\{ \lambda_{U_i} \left[E_{B_i} + \beta_i \left(\frac{b}{2} + y_1 \right)^3 - \varphi_{U_i} - \eta_{U_i} y_1 - \omega_{U_i} y_1^2 \right] + \frac{\delta_{U_i}}{4} \lambda_{U_i}^4 - \frac{\mu_{U_i}}{2} (\rho_{U_i} + \gamma_{U_i} y_1) - \frac{\zeta_i}{3} \phi_i \right\}. \tag{47}$$

Formula (47) expresses the distribution of the J-integral value along the delamination crack front. The average value of the J-integral along the delamination crack front is written as

$$J_{av} = \frac{1}{b} \int_{-\frac{b}{2}}^{\frac{b}{2}} J \, dy_1 \tag{48}$$

It should be mentioned that the J-integral solution derived by substituting of (47) in (48) is exact match of the expression for the strain energy release rate (38). This fact is a verification of the delamination fracture analysis developed in the present paper.

3. NUMERICAL RESULTS

The effects of material gradients and crack location along the height of the cross-section of the beam on the delamination fracture behavior of the multilayered two dimensional functionally graded beam configuration are evaluated.

For this purpose, calculations of the strain energy release rate are carried-out by using formula (38). In order to analyze the influence of the delamination crack location along the height of the beam cross-section on the strain energy release rate, two three-layered beam configurations are considered (Fig. 4). A delamination crack is located between layers 2 and 3 in the beam configuration shown in Fig. 4(a). Fracture behavior of a three-layered beam with a delamination crack between layers 1 and 2 is also investigated (Fig. 4(b)). The thickness of each layer in the two beam configurations is t_l (Fig. 4). In the calculations, it is assumed that b = 0.025 m, t_l = 0.002 m, h = 0.003 m, F = 50 N and t = 1. The material gradient along the width of layer 3 is characterized by E_{D_3}/E_{B_3} ratio. It should be mentioned that E_{B_3} is kept constant in the calculations. Thus, E_{D_3} is varied in order to generate various E_{D_3}/E_{B_3} ratios. It is assumed that E_{B_1}/E_{B_3} = 1.3, E_{D_1}/E_{B_1} = 0.8, E_{H_1}/E_{B_1} = 1.4, E_{B_2}/E_{B_3} = 0.5, E_{D_2}/E_{B_2} = 1.5, E_{H_2}/E_{B_2} = 1.6 and E_{H_3}/E_{B_3} = 1.2. The strain energy release rate is presented in non-dimensional form by using the formula $G_N = G/(E_{B_3}b)$. Calculations are performed for both beam configurations shown in Fig. 4. The strain energy re-

https://doi.org/10.1017/jmech.2017.104 Published online by Cambridge University Press

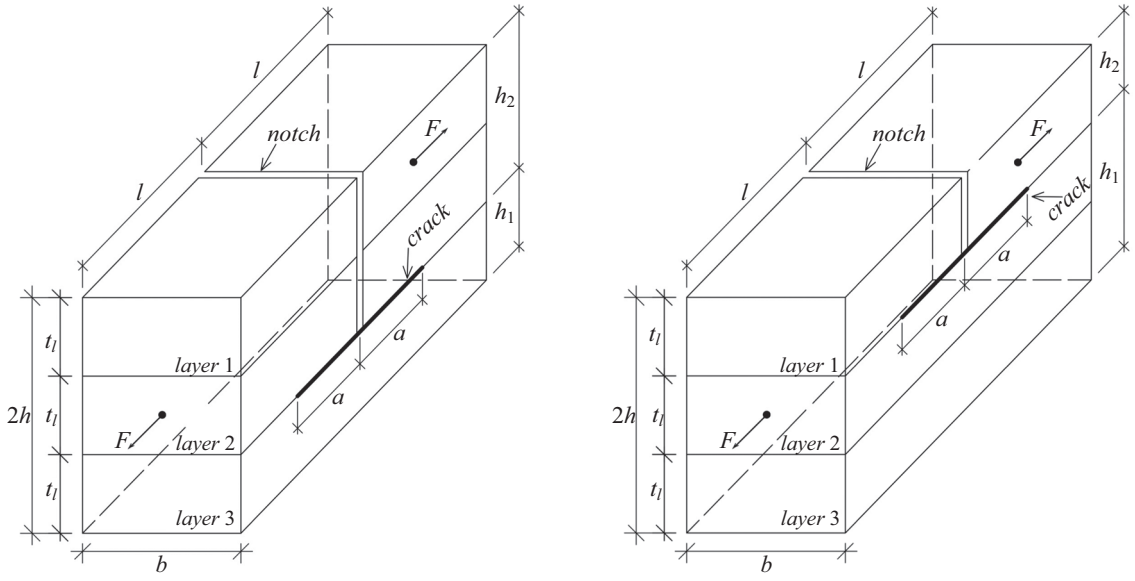


Fig. 4 Schematic representation of two three-layered functionally graded beam configurations.

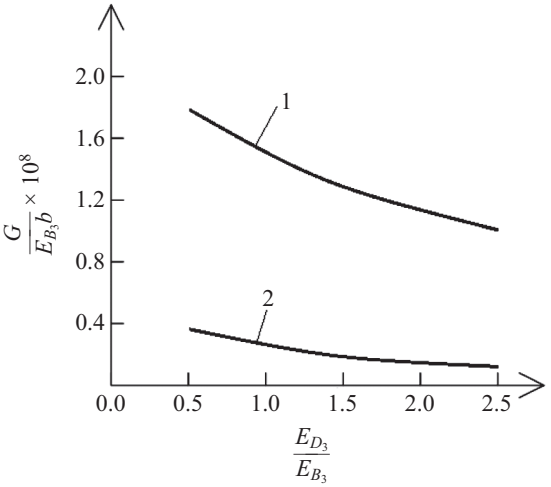


Fig. 5 Figure caption here. Variation of the strain energy release rate in non-dimensional form with respect to E_{D_3}/E_{B_3} ratio (curve 1 – for the three-layered beam configuration shown in Fig. 4(a), curve 2 – for the three-layered beam configuration shown in Fig. 4(b)).

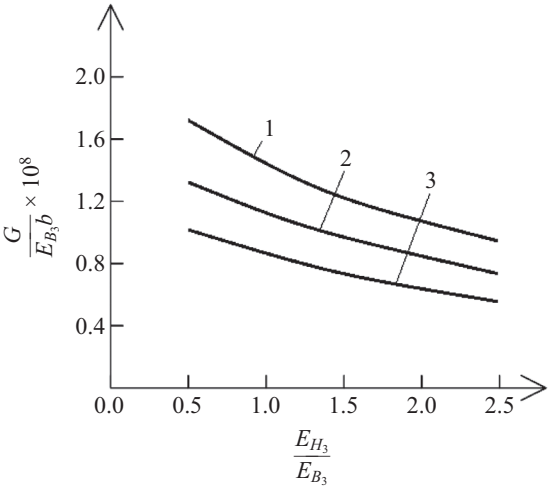


Fig. 6 Variation of the strain energy release rate in non-dimensional form with respect to E_{H_3}/E_{B_3} ratio (curve 1 - at E_{B_2}/E_{B_3} = 0.5, curve 2 - at E_{B_2}/E_{B_3} = 1 and curve 3 - at E_{B_2}/E_{B_3} = 2).

lease rate in non-dimensional form is plotted against E_{D_3}/E_{B_3} ratio in Fig. 5. The curves in Fig. 5 indicate that the strain energy release rate decreases with increasing of E_{D_3}/E_{B_3} ratio. This finding is attributed to the increase of the beam stiffness. One can also observe in Fig. 5 that the strain energy release rate decreases when the delamination crack location is changed from this in Fig. 4(a) to that in Fig. 4(b) (this is due to the increase of the lower crack arm thickness).

The influence of the material gradient along the thickness of layer 3 on the strain energy release rate is also investigated. The material gradient along the thickness of layer 3 is characterized by E_{H_3}/E_{B_3} ratio. In the calculations, E_{B_3} is kept constant. Therefore, various E_{H_3}/E_{B_3} ratios are achieved by varying E_{H_3}.

The beam configuration shown in Fig. 4(a) is analyzed. The strain energy release rate in non-dimensional form is presented as a function of E_{H_3}/E_{B_3} ratio in Fig. 6 at E_{D_3}/E_{B_3} = 0.6. It can be observed in Fig. 6 that the increase of E_{H_3}/E_{B_3} ratio leads to decrease of the strain energy release rate. Besides at E_{B_2}/E_{B_3} = 0.5, the strain energy release rate is analyzed also at E_{B_2}/E_{B_3} = 1 and

https://doi.org/10.1017/jmech.2017.104 Published online by Cambridge University Press

E_{B_2}/E_{B_3} = 2 in order to evaluate the effect of material property, E_{B_2}, on the delamination fracture behaviour of the beam configuration shown in Fig. 4(a). The strain energy release rate obtained at E_{B_2}/E_{B_3} = 1 and E_{B_2}/E_{B_3} = 2 is plotted against E_{H_3}/E_{B_3} ratio in Fig. 6. One can observe in Fig. 6 that the strain energy release rate decreases with increasing of E_{B_2}/E_{B_3} ratio.

4. CONCLUSIONS

An analytical study of delamination fracture in multilayered two-dimensional functionally graded beam configurations exhibiting non-linear mechanical behavior of the material is carried-out. The loading consists of two longitudinal forces applied at the free ends of the beam. A delamination crack is located symmetrically with respect to the beam mid-span. The fracture behavior is studied in terms of the strain energy release rate. The solution derived is verified by the *J*-integral approach. The solution can be applied to calculate the strain energy release rate in beams made of an arbitrary number of layers. Besides, the delamination crack is located arbitrary along the height of the beam cross-section. The layers have different thicknesses and material properties. Also, the material is two-dimensional functionally graded in the cross-section of each layer. The solution derived is applied to evaluate the effects of material gradients and crack location along the height of the beam cross-section on the delamination fracture behavior. The analysis reveals that the strain energy release rate decreases with increasing of E_{D_3}/E_{B_3} and E_{H_3}/E_{B_3} ratios. It is found also that the increase of the lower crack arm thickness leads to decrease of the strain energy release rate. The analysis developed in the present paper can be applied to optimize the multilayered two-dimensional functionally graded beam structures with respect to their delamination fracture performance. For instance, the results obtained indicate that the strain energy release rate can be efficiently regulated by employing appropriate material gradients in the design stage of beam structures.

NOMENCLATURE

A	Crack area, m^2;
a	Crack length, m;
b	Beam width, m;
E_i	Material property, Pa;
F	External force, N;
G	Stain energy release rate, J/m^2;
h	Beam height, m;
J	*J*-integral, J/m^2;
L	Beam length, m;
M_{y_1}	Bending moment about y_1 centroidal axis, Nm;
M_{z_1}	Bending moment about z_1 centroidal axis, Nm;
N_1	Axial force, N;
n	Number of layers;
p_{x_i}	Component of the stress vector, Pa;
p_{y_i}	Component of the stress vector, Pa;
ds	Differential element along the contour of integration, m;
t	Material property;
t_l	Thickness of a layer, m;
U^*	Complementary strain energy, J;
u	Component of the displacement vector, m;
u_0	Strain energy density, J/m^3;
u_0^*	Complementary strain energy density, J/m^3;
v	Component of the displacement vector, m;
W_{ext}	Work of external forces, J;
x_1	Centroidal axis, m;
y_1	Centroidal axis, m;
z_1	Centroidal axis, m;
α	Angle between the outwards normal vector to the contour of integration and the crack direction;
ε	Longitudinal strain;
Γ	Contour of integration, m;
κ_{y_1}	Curvature of lower crack arm in x_1y_1 plane, 1/m;
κ_{z_1}	Curvature of lower crack arm in x_1z_1 plane, 1/m;
σ_i	Longitudinal normal stress, Pa.

REFERENCES

1. Koizumi, M., "The Concept of FGM Ceramic Trans.," *Functionally Gradient Materials*, **34**, pp. 3-10 (1993).
2. Suresh, S. and Mortensen, A., *Fundamentals of Functionally Graded Materials*, IOM Communications Ltd, London (1998).
3. Levashov, E. A. *et al*., "Self-Propagating High-Temperature Synthesis of Functionally Graded PVD Targets with a Ceramic Working Layer of TiB-TiN or TiSi-Tin," *Journal of Materials Synthesis and Processing*, DOI: 10.1023/A:1023881718671 (2002).
4. Tokova, L., Yasinskyy, A. and Ma, C.-C., "Effect of the Layer Inhomogeneity on the Distribution of Stresses and Displacements in an Elastic Multilayer Cylinder," *Acta Mechanica*, DOI: 10.1007/s00707-015-1519-8 (2016).
5. Tokovyy, Y. and Ma, C.-C., "Three-Dimensional Temperature and Thermal Stress Analysis of an Inhomogeneous Layer," *Journal of Thermal Stresses*, **36**, pp. 790-808 (2013).
6. Tokovyy, Y. and Ma, C.-C., "Axisymmetric Stresses in an Elastic Radially Inhomogeneous Cylinder Under Length-Varying Loadings," *ASME Journal of Applied Mechanics*, DOI: 10.1115/1.4034459 (2016).

https://doi.org/10.1017/jmech.2017.104 Published online by Cambridge University Press

7. Uslu Uysal, M. and Kremzer, M., "Buckling Behaviour of Short Cylindrical Functionally Gradient Polymeric Materials," *Acta Physica Polonica*, **A127**, pp. 1355-1357 (2015).
8. Uysal, M. U., "Buckling Behaviours of Functionally Graded Polymeric Thin-Walled Hemispherical Shells, Steel and Composite Structures," *An International Journal*, **21**, pp. 849-862 (2016).
9. Maalawi, K. Y., "Dynamic Optimization of Functionally Graded Thin-Walled Box Beams," *International Journal of Structural Stability and Dynamics*, https://doi.org/10.1142/S0219455417501097 (2017).
10. George, N., Jeyaraj, P. and Murigendrappa, S. M., "Buckling and Free Vibration of Nonuniformly Heated Functionally Graded Carbon Nanotube Reinforced Polymer Composite Plate," *International Journal of Structural Stability and Dynamics*, https://doi.org/10.1142/S021945541750064X (2017).
11. Nejad, M. Z., Hoseini, Z., Niknejad, A. and Ghannad, M., "Steady-State Creep Deformations and Stresses in FGM Rotating Thick Cylindrical Pressure Vessel," *Journal of Mechanics*, **31**, pp. 1-6 (2017).
12. Paulino, G. C., "Fracture in Functionally Graded Materials," *Engineering Fracture Mechanics*, **69**, pp. 1519-1530 (2002).
13. Tilbrook, M. T., Moon, R. J. and Hoffman, M., "Crack Propagation in Graded Composites," *Composite Science and Technology*, **65**, pp. 201-220 (2005).
14. Carpinteri, A. and Pugno, N., "Cracks in Re-Entrant Corners in Functionally Graded Materials," *Engineering Fracture Mechanics*, **73**, pp. 1279-1291 (2006).
15. Upadhyay, A. K. and Simha, K. R. Y., "Equivalent Homogeneous Variable Depth Beams for Cracked FGM Beams; Compliance Approach," *International Journal of Fracture*, **144**, pp. 209-213 (2007).
16. Panigrahi, B. and Pohit, G., "Nonlinear Modelling and Dynamic Analysis of Cracked Timoshenko Functionally Graded Beams Based on Neutral Surface Approach," *Proceedings of the Institution of Mechanical Engineers, Part C: Journal of Mechanical Engineering Science*, **230**, pp. 1468-1497 (2016).
17. Zhang, H., Li, X. F., Tang, G. J. and Shen, Z. B., "Stress Intensity Factors of Double Cantilever Nanobeams via Gradient Elasticity Theory," *Engineering Fracture Mechanics*, **105**, pp. 58-64 (2013).
18. Pan, S.-D., Feng, J.-C., Zhou, Z.-G. and Zhi, W.-L., "Four Parallel Non-Symetric Mode –III Cracks with Different Lengths in a Functionally Graded Material Plane," *Strength, Fracture and Complexity: an International Journal*, **5**, pp. 143-166 (2009).
19. Monfared, M. M., Ayatollahi, M. and Mousavi, S. M., "The Mixed-Mode Analysis of Functionally Graded Orthotropic Half-Plane Weakened by Multiple Curved Cracks," *Archive of Applied Mechanics*, **86**, pp. 713-728 (2016).
20. Uysal, M. U. and Güven, U., "A Bonded Plate Having Orthotropic Inclusion in Adhesive Layer under In-Plane Shear Loading," *The Journal of Adhesion*, **92**, pp. 214-235 (2016).
21. Dahan, I., Admon, U., Sarei, J. and Yahav, B., "Amar, M., Frage, N. and Dariel, M. P., Functionally Graded Ti-TiC Multilayers: the Effect of a Graded Profile on Adhesion to Substrate," *Materials Science Forum*, **308-311**, pp. 923-929 (1999).
22. Hosseini Hashemi, Sh. and Bakhshi Khaniki, H., "Dynamic Behavior of Multi-Layered Viscoelastic Nanobeam System Embedded in a Viscoelastic Medium with a Moving Nanoparticle," *Journal of Mechanics*, **33**, pp. 559-575 (2017).
23. Gupta, S. and Bhengra, N. "Dispersion Study of Propagation of Torsional Surface Wave in a Layered Structure," *Journal of Mechanics*, **33**, pp. 303-315 (2017).
24. Yildirim, B., Yilmaz, S. and Kadioglu, S., "Material Coatings under Thermal Loading," *Journal of Applied Mechanics*, **75**, 051106 (2008).
25. Dolgov, N. A., "Determination of Stresses in a Two-Layer Coating," *Strength of Materials*, **37**, pp. 422-431 (2005).
26. Dolgov, N. A., "Analytical Methods to Determine the Stress State in the Substrate–Coating System under Mechanical Loads," *Strength of Materials*, **48**, pp. 658-667 (2016).
27. Choi, S. R., Hutchinson, J. W. and Evans, A. G., "Delamination of Multilayer Thermal Barrier Coatings," *Mechanics of Materials*, **31**, pp. 431-447 (1999).
28. Szekrenyes, A., "Semi-Layerwise Analysis of Laminated Plates with Nonsingular Delamination - The Theorem of Autocontinuity," *Applied Mathematical Modelling*, **40**, pp. 1344-1371 (2016).
29. Szekrenyes, A., "Nonsingular Crack Modelling in Orthotropic Plates by Four Equivalent Single Layers," *European Journal of Mechanics – A/Solids*, **55**, pp. 73-99 (2016).
30. Ivanov, I. and Draganov, I., "Influence and Simulation of Laminated Glass Subjected to Low-Velocity Impact," *Mechanics of Machines*, **110**, pp. 89-94 (2014).
31. Ivanov, V., Velchev, D. S., Georgiev, N. G., Ivanov, I. D. and Sadowski, T., "A Plate Finite Element for Modelling of Triplex Laminated Glass and Comparison with Other Computational Models," *Meccanica*, **51**, pp. 341-358 (2016).
32. Chakrabarty, J., *Theory of Plasticity*, Elsevier Butterworth-Heinemann, Oxford (2006).
33. Lubliner, J., *Plasticity Theory (Revised Edition)*, University of California, Berkeley (2006).
34. Petrov, V. V., *Non-Linear Incremental Structural Mechanics*, M., Infra-Injeneria, Moscow (2014).

https://doi.org/10.1017/jmech.2017.104 Published online by Cambridge University Press

35. Broek, D., *Elementary Engineering Fracture Mechanics*, Springer, Berlin (1986).

(Manuscript received June 24, 2017,
accepted for publication October 4, 2017.)

https://doi.org/10.1017/jmech.2017.104 Published online by Cambridge University Press